ILASS Americas 26th Annual Conference on Liquid Atomization and Spray Systems, Portland, OR, May 2014

High-Fidelity Simulation of Atomization in a Gas Turbine Injector High Shear Nozzle

D. Kim *, F. Ham and H. Le
Cascade Technologies, INC
2445 Faber Pl. Suite 100, Palo Alto, CA 94303

M. Herrmann
Arizona State University, Tempe, AZ 85281

X. Li, M. C. Soteriou and W. Kim
United Technologies Research Center, Wast Hartford, CT 06108

Abstract

The details of liquid atomization and the resulting spray formation processes in realistic complex fuel injectors are not well understood, because experimental access to the atomization region is typically severely limited, if not outright impossible. A significant portion of the atomization process occurs in spatial regions adjacent to solid walls that block experimental access into the injector so that experimental studies are limited to either far field measurements of complex injectors, after most of the atomization has occurred, or to simple injector geometries such as a circular cross-section pipes injecting into crossflow channels. Due to recent advances in numerical methods and available computational resources, high-fidelity simulations of the atomization process are starting to emerge as an alternative to experimental studies for understanding and predicting the spray formation process. In the present study, a novel unstructured Volume-of-Fluid (VoF) method coupled to a Lagrangian spray approach is employed to simulate the atomization process in a realistic high shear nozzle typical of gas turbine injectors, consisting of six liquid jets injecting into a crossflow swirling gaseous nozzle flow. Simulations are performed at ambient conditions and compared to experimental data of the resulting spray at different far field measurement planes downstream of the nozzle.

*Corresponding Author: dkkim@cascadetechnoloigies.com

1 Introduction

To understand the atomization of liquid fuel in air stream is important to design injector system in gas turbine engines for high performance. The primary breakup process near injectors which yields droplets in the far field has substantial influence on combustion efficiency of the gas turbine engines. However, the details of atomization process in realistic complex fuel injectors are not well understood because experimental access to the primary atomization region near injectors is very limited in complicated geometric design. Thus, the experimental data are often restricted to far-field measurement where most of the atomization has already occurred.

Numerical modeling of atomization process is also challenging because of complex and multi-scale characteristics ranging from millimeters to microns. Two-phase flows are generally classified into three regimes according to the shape of the interface: separated flows, dispersed flows, and mixed flows. In dispersed flows, one phase is assumed to be dilute and the dispersed dilute phase is often treated in a Lagrangian way. The droplets are assumed as point particles because the particle size is very small as compared to the macroscopic scale. The individual particles are tracked by solving Newton's second law considering the forces acting on the particles. The flow inside the particles does not need to be solved and the interaction between flow and particles is taken into account by adding source terms in the Navier-Stokes equations. Many numerical models have been proposed and validated for turbulent particle flows in dilute phase [1, 2, 3, 4]. However, the Lagragian approach is inaccurate for atomization process in the mixed regime where breaking or merging frequently occurs.

To accurately simulate the interface breaking or merging, the phase interface should be tracked or captured numerically. Among several phase-tracking methods based on the Eulerian approach, the level set method [5] and the volume-of-fluid (VoF) method [6] are popular. Although the level-set method can handle topology changes automatically, its main drawback is the volume conservation is not inherently guaranteed. The VoF method shows better volume conservation, but requires a specific advection scheme for the transport equation of VoF scalar, thereby affecting the accuracy of the scheme and volume conservation. Moreover, calculating geometric quantities such as surface normal and curvature remains problematic. In order to overcome weaknesses, the refined level-set grid (RLSG) method [7] and the coupled level-set and volume-of-fluid (CLSVOF) method [8] have been developed.

Due to recent advances in numerical methods and available computational resources, high-fidelity simulations on atomization are starting to emerge as an alternative to experimental studies for understanding breakup and predicting the spray formation process. However, a number of challenges must be overcome to perform multiphase flow simulations for realistic atomization in a complex fuel injector. First of all, mass conservation should be guaranteed because even a small numerical diffusion error in each phase mass is critical to the small-size drops. Thus, 100% mass conservation is necessary to maintain fine sprays in the mixed two-phase flow where the separated and dispersed phase coexist. In addition to the mass conservation, one must ensure solver robustness at realistic density ratios. It is also challenging to reduce the computational cost while providing successful modeling of multiphase flows. In the area of high-performance computing, achieving speed and scalability is complicated by the highly dynamic workload associated with the moving interface, as well as the variable coefficient unstructured Poisson system that must be solved in each time step. Finally, injector geometries of engineering interest are complex, and are modeled most efficiently using unstructured or hybrid-structured grids.

In the present study, we coupled a novel unstructured Volume-of-Fluid (VoF) method [9] to a Lagrangian spray approach to simulate atomization of liquid fuel in a realistic high shear nozzle of typical gas turbine injectors. The VoF-based scheme is geometric and un-split, allowing exact mass conservation and addressing the challenges mentioned above: robust handling of high-density ratios, integrating and testing a droplet transfer algorithm with exact mass conservation, and solving the variable-coefficient Poisson system. We have simulated a realistic fuel atomization process in a swirling injector, consisting of six liquid jets injecting into a crossflow swirling gaseous nozzle flow. At first, the simulations were performed on a 30-degree sector of the swirling injector with one liquid injector. The grid adaptation near the injector and the liquid jet structure are presented in this paper. Finally, numerical simulations are performed for full six liquid nozzles and compared to experimental data of the resulting spray done by United Technologies Research Center (UTRC) [10] at a far field measurement plane downstream of the nozzle.

2 Unstructured VoF scheme

The Navier-Stokes equations for incompressible, immiscible, two-phase flow are described as

$$\frac{\partial \rho}{\partial t} + \frac{\partial \rho u_j}{\partial x_j} = 0, \tag{1}$$

$$\frac{\partial u_j}{\partial x_j} = 0, \tag{2}$$

$$\frac{\partial \rho u_i}{\partial t} + \frac{\partial \rho u_i u_j}{\partial x_j} = -\frac{\partial p}{\partial x_i} + \frac{\partial}{\partial x_j}\mu\big(\frac{\partial u_i}{\partial x_j} + \frac{\partial u_j}{\partial x_i}\big) + T_i, \tag{3}$$

where ρ is the density, μ the viscosity, p the pressure, u_i the velocity, and T_i is the surface tension force. Assuming ρ and μ are constant within each phase, the density and viscosity are defined as a function of VoF, ψ:

$$\rho = \psi\rho_1 + (1-\psi)\rho_2, \tag{4}$$
$$\mu = \psi\mu_1 + (1-\psi)\mu_2, \tag{5}$$

where the subscripts 1 and 2 denote properties in fluid 1 and 2, respectively. In the present method, we follow the Piecewise-Linear Interface Calculation (PLIC) scheme where a plane is located geometrically within the control volume and oriented in the direction of the local surface normal. PLIC method has a clear advantage in conserving mass and constructing monotone advection scheme because the mass flux can be calculated geometrically from the plane of phase interface. At present, the required surface normal is computed based on an upwinded advection of the previous signed distance field to the interface, although alternative approaches based directly on the VoF scalar are being considered. The implicit location of the plane is determined using a bisection/secant algorithm that locates the fluid level in each control volume. The result of this step is stored as a single scalar value representing the signed distance of the interface from the node. VoF equation 1 is solved by integrating the upwind side of flux volume which will be fluxed across the flux face during δt. The flux volume is selected based on the velocity on the face to avoid the overlap of the flux volume from the other flux face. Once the VoF scalar is updated, the mass flux is computed directly from this VoF advection and also used in a consistent way in the momentum discretization, resulting in a perfectly mass-conserving, un-split, monotonic, unstructured VoF scheme that is stable at large density ratios. The details of the numerical method and validations are described in [9].

3 Eulerian-Lagrangian coupling

In our simulation approach, we propose to simulate the initial breakup process of the injected liquid in detail using the VoF approach, resolving the dynamics of the phase interface including topology change events. However, due to the large number of droplets generated in the atomization process, the corresponding phase interface surface area quickly becomes too large to resolve even when using the largest computational resources available today. For small scale droplets where the local Weber number is close to unity, surface tension forces are dominant, resulting in droplet shapes that are predominantly spherical without significant deviations from this form. Standard Lagrangian particle modeling approaches are thus applicable and provide for a significantly more efficient way to model these droplets than resolving their phase interface dynamics using a VoF approach.

The Lagrangian liquid particle motion is simulated using Basset-Boussinesq-Oseen (BBO) equations [11]. It is assumed that the density of the particle is much larger than that of the gaseous fluid (O[1000]), that the particle size is small compared with the turbulence integral length scale, and that the effect of shear on the particle motion is negligible. The large density ratio means that the Basset force and the added mass term are small and, therefore, are neglected. Under these assumptions, the particle motion is governed by the Lagrangian equations:

$$\frac{dx_p}{dt} = u_p, \tag{6}$$

$$\frac{du_p}{dt} = D_p(u - u_p) + \Big(1 - \frac{\rho_g}{\rho_l}\Big)g, \tag{7}$$

where u_p and u are the particle velocities and gas phase velocities at the particle location, respectively. ρ_g and ρ_l are the particle and gas densities, respectively. g is the gravitational acceleration. The drag force on the particle is modeled by a drag coefficient C_d [11] as

$$D_p = \frac{3}{4}C_d\frac{\rho_g}{\rho_l}\frac{|u-u_p|}{d_p}, \tag{8}$$

where d_p is the particle diameter.

The further breakup of Lagrangian particles into smaller drops is modeled by a stochastic breakup model, in which the characteristic radius of drops is assumed to be a time-dependent stochastic variable with a given initial-size distribution [4]. The

breakup of a parent drop is viewed as the temporal and spatial evolution of this distribution function around the parent-drop size, according to the Fokker-Planck differential equation. This distribution function follows a certain long-time behavior, which is characterized by the dominant mechanism of breakup.

$$\frac{\partial T(x,t)}{\partial t} + \nu(\xi)\frac{\partial T(x,t)}{\partial x} = \frac{1}{2}\nu(\xi^2)\frac{\partial^2 T(x,t)}{\partial x^2}, \quad (9)$$

where ν the breakup frequency. Here, $T(x,t)$ is the distribution function for $x = \log(r_j)$, where r_j is the droplet radius. Breakup occurs when $t > t_{breakup} = 1/\nu$, where the aerodynamics force are balanced with surface tension force. The satellite sub-droplets from mother drops are sampled from the analytical solution of Eq. 9 corresponding to the breakup timescale. When new satellite drops are formed, mother drops are deleted. Lagrangian tracking for new drops is continued until further breakup happens. The stochastic breakup stops when the size of drops reaches the critical (or maximum stable) radius for breakup where the hydrodynamic force is balanced by capillary force:

$$r_{cr} = \frac{We_{cr}\sigma}{\rho_g(u-u_p)^2}, \quad (10)$$

where the critical Weber number, We_{cr}, is chosen to be six based on a wide range of experiments [12, 13].

In order to couple both approaches, the Eulerian VoF approach to resolve the phase interface dynamics during primary breakup and the Lagrangian based approach for the subsequent spray evolution, we follow the procedure described in [14] but adapt it to using a volume of fluid scalar on fully unstructured meshes instead of a level set scalar on banded structured meshes.

The resulting Eulerian-Lagrangian coupling algorithm consists of the following steps:

1. Mark all mesh edges where at least one of the corresponding nodes has a volume fraction greater than a small threshold value ϵ (typically $\epsilon = 10^{-12}$).

2. Tag all nodes that have at least one edge marked in the previous step and reduce the tag identification of jointly marked node-edge combinations to a globally unique number. This step ensures that continuous liquid structures surrounded entirely by nodes with volume fraction less than ϵ are tagged with a unique identifier.

3. Calculate liquid volume and shape metrics for each uniquely identified liquid structure and select those that have volume smaller than a set threshold volume proportional to the local mesh size, and are of near spherical shape (see [14] for further details).

4. Reset the volume fraction of all nodes belonging to the selected structures to zero, thereby removing them from the Eulerian representation, and insert Lagrangian point particles in their place preserving their mass, momentum, and location of their center of mass.

# drops	60 procs	120 procs
1000	0.30s	0.16s
25,000	1.59s	0.78s

Table 1. Wall clock timing results for parallel Eulerian-Lagrangian transfer algorithm.

Table 1 shows timing results for the Eulerian-Lagrangian transfer algorithm executed for 1000 and 25,000 randomly placed mono disperse droplets inside a unit sized cube. As demonstrated, the algorithm is both fast and scalable. Figure 1 shows the transferred (white) and non-transferred (blue) liquid structures for 5,000 respectively 25,000 randomly placed mono-disperse droplets. As shown, almost all droplets are identified and transferred in the 5,000 droplet case, whereas only a small number are transferred in the 25,000 droplet case. This is due to the fact that when placing 25,000 droplets randomly inside a unit sized cube, a significant number of droplets partially overlap, creating joined structures that do not satisfy the transfer criterium described in step 3. Placing only 5,000 droplets, on the other hand, most drops are isolated and thus are transferred. This behavior is consistent with the one observed in [14].

4 Numerical Simulation of a Swirling Injector

In this section we present numerical simulations of a realistic fuel atomization process in a complex combustor/augmentor fuel injector. In order to investigate the primary atomization of the injected liquid fuels and their subsequent secondary breakup, the unstructured VoF-based scheme is applied, coupled to Lagrangian point particle tracking model with multi-physics modeling. The injector geometry is obtained from UTRC [10], where experiments were performed to characterize the droplet size dis-

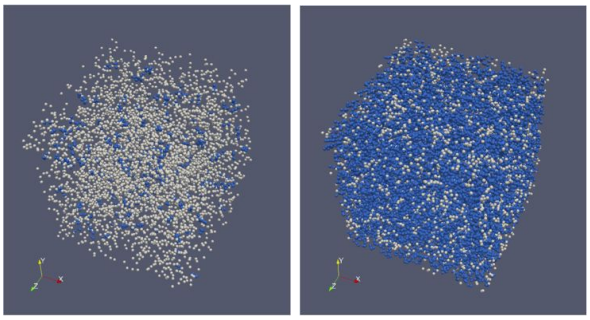

Figure 1. Eulerian-Lagrangian transfer algorithm applied to 5,000 (left) and 25,000 (right) randomly placed mono-disperse drops. Transferred drops are shown in white, non-transferred drops remaining in the VoF representation are shown in blue.

tribution produced by the injector at ambient conditions.

4.1 Simulation of a 30-Degree Sector of the Swirling Injector

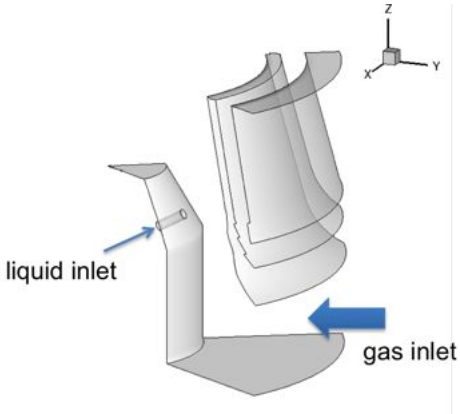

Figure 2. Geometric configuration of a 30-degree sector of the swirling injector.

To better understand the flow and interface structures and resolution requirements associated with the high-shear injector, a single nozzle simulation was initiated and the results are shown below. Instead of the full circumference of the injector, we initially restrict this simulation to a 30 degree azimuthal sector of the injector in order to decrease the computational costs, although there is no experimental data available for a 30-degree sector case. The purpose of this simulation is the demonstration of a realistic two-phase flow computation and to gain experience in the setup, execution and post-processing of the multiphase computations. Figure 2 shows the geometric configuration of the single injector showing gas and liquid inlets. For the gas, the inlet velocity is $100m/s$ and the density and viscosity are set to $1.2kg/m^3$ and 1.8×10^{-5}, respectively. For the liquid, the inlet velocity, density and viscosity are $18m/s$, $780kg/m^3$ and 1.5×10^{-3}, respectively. The surface tension coefficient used is $0.024N/m$. The diameter of the injector, D, is $0.64mm$. In the case of the unstructured grids in the present simulation, cell resolution and aspect ratio can vary rapidly in space. Before running the main simulation, the preliminary simulation with coarse grid resolution was performed to obtain the liquid jet trajectory so that the grid can be adaptively refined following the trajectory before the final simulation. The adaptive grid refinement in the final simulation results in a total sector grid size of 10.5 million as shown in Fig. 3. 300 CPUs of Intel Westmere-EP are used in the simulation and it takes 6 days in CPU hours to reach 0.0015 seconds in physical time.

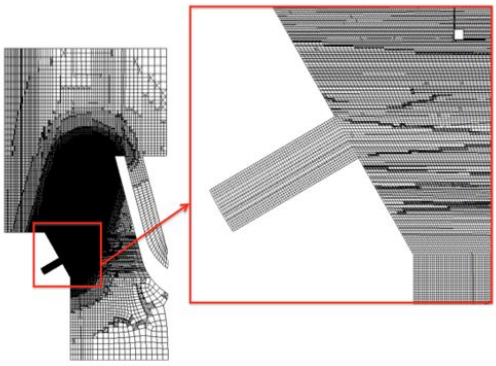

Figure 3. Details of grid adaptation near the injector.

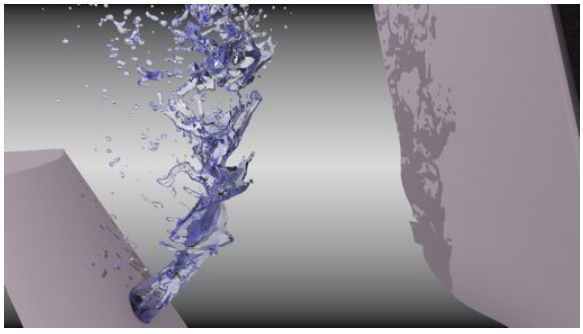

Figure 4. Structure of the liquid jet near the injector.

The simulation was first performed without coupling to Lagrangian particle approach with the Stochastic breakup model. Figure 4 shows the identification of phase interface structure associated with the primary atomization. Visualization is based on an isosurface of VoF=0.5. Liquid drops are stripped off from the liquid jet core by high-shear gas flow right after injection. The liquid core then undergoes modulation and eventually breaks up into liquid blobs and sheets.

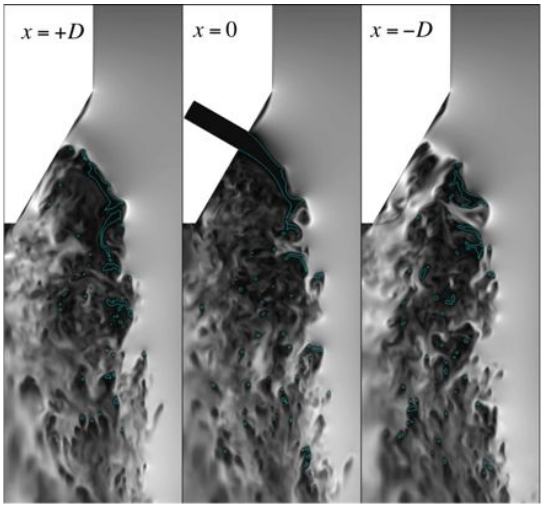

Figure 5. Contours of the velocity magnitude at different positions in x direction. $D = 0.64mm$ is the diameter of the injector.

The contours of velocity magnitude for different locations in x direction are shown in Fig. 5, illustrating details of the interaction between the airstream and the liquid jet and droplets. Here, the center of the injector is located at $x = 0$. The grey scale represent velocity magnitude and the blue line is the liquid interface. The surface instability is found on the liquid jet core, which results in the liquid blobs and droplets. The wake is clearly observed behind the liquid droplets so that it substantially affects the air flow.

Figures 6 and 7 show the isosurface of VoF without and with Lagrangian stochastic breakup model, respectively. In Fig. 7, the isosurface of VoF and Lagrangian particles are presented in green and blue colors, respectively. It is observed that lots of subgrid Lagrangian drops are generated by stochastic breakup model, which will be further broken into smaller drops until their size is smaller than the critical radius. Validity of stochastic breakup model will be discussed in the next section.

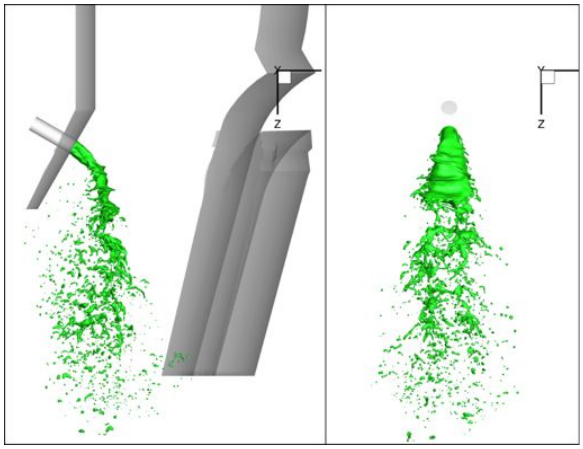

Figure 6. Isosurface of VoF without the Lagrangian stochastic breakup model.

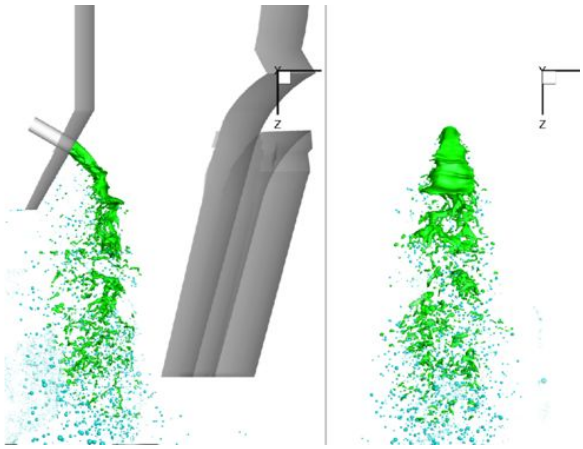

Figure 7. Isosurface of VoF with Lagrangian stochastic breakup model. Green: isosurface; blue: Lagrangian particle.

4.2 Full Simulation of the entire Swirling Injector

In order to validate our numerical method, a full circumference of the fuel injector with six liquid inlets was simulated and compared with the experiment [10]. The details of the nozzle are shown in Fig. 8 and geometrical configuration of the swirler is illustrated in Fig. 9. The liquid fuel is injected at six nozzles inside the inner swirler. The atomization of liquid jet occurs mostly due to the cross swirling flow in the inner swirler. Large liquid chucks or droplets are further atomized by the secondary outer swirling flow. These two subsequent processes yield fine fuel droplets, which are well mixed with air by the strong swirling flow in the downstream of the injector.

The operating condition is set to be same as the

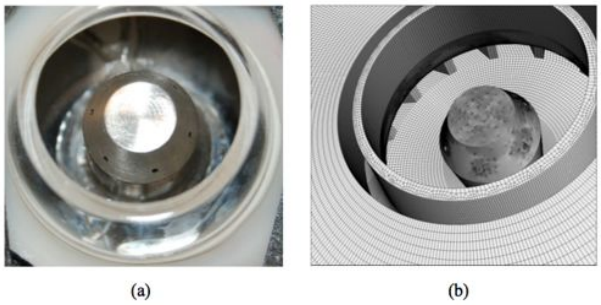

Figure 8. Details of liquid fuel nozzles: (a) experiment [10]; (b) simulation.

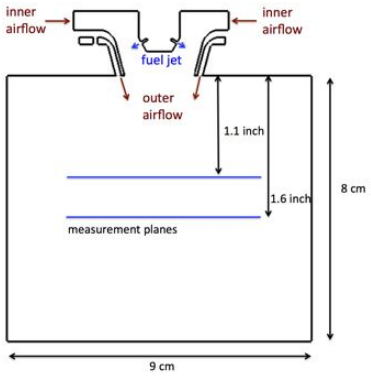

Figure 9. Configuration of the swirler system.

experiment from UTRC [10]. The liquid fuel (JET-A) is injected at six nozzles with a total mass flow rate of $0.0125kg/s$. The inlet boundary for air is set to match with air flow rate of $0.044kg/s$ measured in the experiment. Based on an averaged air velocity in the inner swirler passage in the simulation, the momentum flux ratio is about 10 and the corresponding gas Weber number is about 160 in the swirling cross flow. The jet momentum ratio was selected in the experiment as to minimize the amount of jet impingement on the conical surface of the injector, such that the resulting filming and subsequent drop dripping could be avoided at this point in the investigation. The experiment was performed at the ambient condition. For the fuel (JET-A), the density and viscosity are $780kg/m^3$ and $1.53 \times 10^{-3}kg/m/s$ and the air density and viscosity are $1.205kg/m^3$ and $1.77 \times 10^{-5}kg/m/s$, respectively. The surface tension coefficient is $0.024N/m$. The diameter of the injector is set to $0.64mm$ as the experiment.

Figure 10 shows the grids in the full domain,

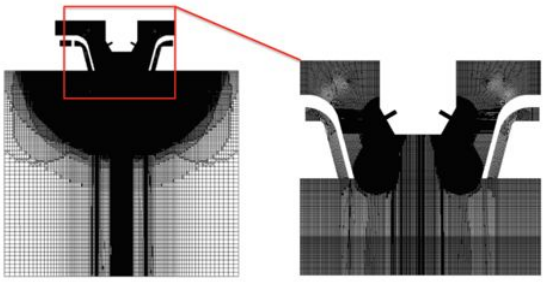

Figure 10. Adaptive grids used in the numerical simulation.

zooming the injector region. The adaptive grid refinement near the injector region yields total 210 million grids. In the experiment [10], the smallest droplet size is measured as $10 \sim 20\ \mu m$. Due to the limit of computational resources, the grid size near the trajectory of liquid column is set to $18\mu m$, which is not enough to fully resolve the smallest droplet measured in the experiment, but comparable size. In order to refine the grid adaptively following the trajectory of liquid jet, the numerical simulation was performed first on coarse grid to obtain preliminary results. The smallest grid size is set to $80\mu m$ in the vicinity of the injector and the total number of grids is then 18 millions in the coarse grid simulation. In every numerical simulation, the small spherical droplets are transferred to Lagrangian point particles based on the Eulerian-Lagrangian coupling algorithm described in section 3. In the present study, the stochastic breakup model [4] is only applied to the coarse grid simulation since the grid size is too large to predict the correct droplet size in the far field. In the experiment, spray statistics are measured at two different locations (Fig. 9). In the present simulations, all liquid droplets in Eulerian description are transferred to Lagrangian particles before reaching the measurement locations. For comparison study, the Lagrangian spray statistics is compared with the experimental data at the first measurement plane located 1.1inch from the injector.

Figure 11 shows the comparison of the liquid jet atomization in the near injector. Lagragian drops transferred from VoF representations are shown in blue spheres in Fig. 11(b), while the VoF iso-surface is depicted in green. The operating conditions for the experiment and simulation are same except the outer swirler cone is removed in the experiment to obtain clear images of the liquid jets inside the swirler cone. Although it is difficult to see the de-

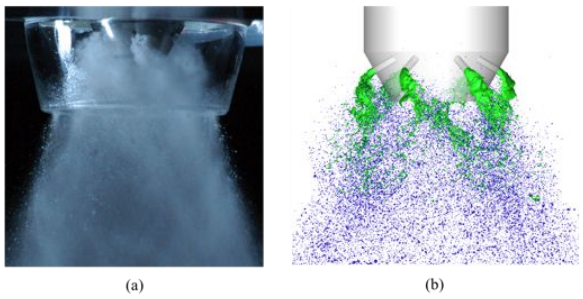

Figure 11. Comparison of liquid fuel atomization in the near injector: (a) experimental photo [10]; (b) present simulation. Green: VoF isosurface; blue: Lagrangian drops.

tails of liquid jet atomization in the experiment since the exposure time is not fast enough to capture a still clear image, the overall shape of liquid jet injection in the simulation (Fig. 11(b)) compares well with the experimental image (Fig. 11(a)) qualitatively. View from the exit of the injector is depicted in Fig. 12 showing the six liquid jets atomized by swirling air flow.

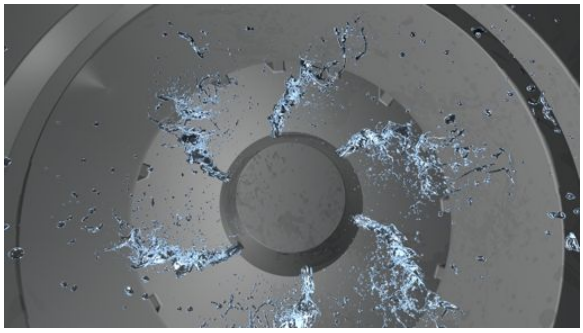

Figure 12. Instantaneous liquid jet structure from the six nozzles viewed from the exit of the swirler.

The liquid droplets generated by the inner swirler are further mixed with air by the outer swirler and spreading in the downstream of the injector. The shape of spreading in simulation in Fig. 13(b) is well matched with the experimental image [10] in Fig 13(a). Since the sufficient number of Lagrangian drops reached the first measurement plane located 1.1 inch from the injector to collect the spray statistics, comparison of spray statistics between the experiment and simulation is done and shown in Fig. 14. The spray statistics is averaged in the circular direction for the Lagrangian droplets crossing the measurement plane. For comparison, the fuel mass flux from the numerical simulation is scaled

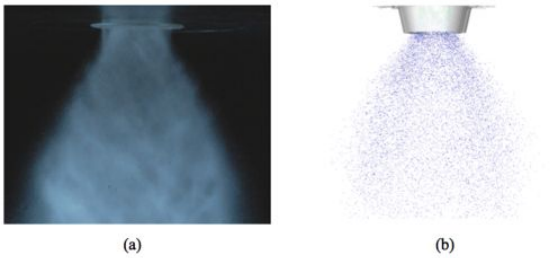

Figure 13. Comparison of the droplet spreading in the far field: (a) experimental photo [10]; (b) present simulation.

to match with the peak value of the scaled experimental data (Fig 14(a)). The location of peak in the fuel mass flux exactly matches with the experimental measurement. The mean axial velocity component of the liquid fuel has also good agreement with the experiment except that the simulation has a higher peak and slightly narrow profile because of the side boundary effect in the numerical simulation (Fig 14(b)).

The Sauter mean diameter (SMD) of the droplets is measured at the same locations and compared in Fig. 15. The SMD of droplets from the coarse grid simulation is depicted together with the fine grid result to investigate the effect of grid resolution on drop-size distribution. For all cases, SMD values are divided by the maximum SMD measured in the experiment [10]. It is observed that the larger droplets are centrifuged out because of the swirling air flow. This characteristic is also found in both simulations. The predicted mean diameter of droplets are larger than the experimental measurement for both grids mostly because both fine grid ($\Delta \sim 18\mu m$) and coarse grid resolution ($\Delta \sim 80\mu m$) are above the smallest droplet size measured in the experiment. However, considering that the fuel flow rates for the inner and outer circular regions are negligible to collect meaningful statistics, where the radius is smaller than 0.5 inch or larger than 1.0 inch, the numerical prediction is well matched with the experimental data even for the coarse grid. This demonstrates the potential benefit of the Lagrangian stochastic breakup model [4] when the grid resolution is too coarse to resolve the fine sprays, which is likely to happen in most of practical engineering cases.

5 Conclusion

A novel unstructured VoF scheme has been developed and coupled with a Lagrangian approach for describing secondary droplets and secondary

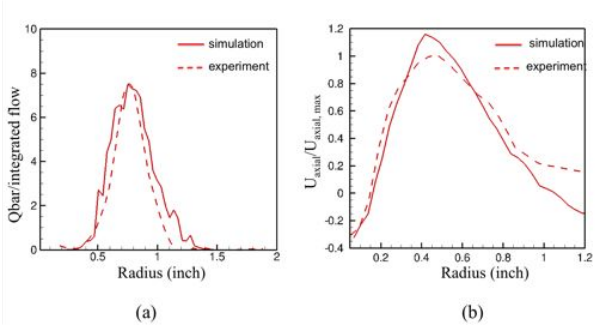

Figure 14. Comparison of spray statistics at the 1.1 inch measurement plane: (a) scaled circular averaged mass flux; (b) circular averaged axial velocity component of liquid droplets.

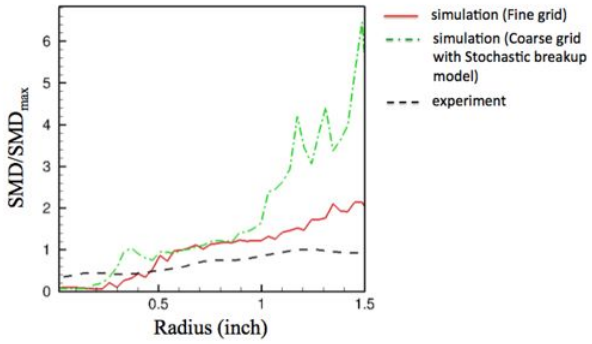

Figure 15. Comparison of the Sauter mean diameter (SMD) of droplets at the 1.1 inch measurement plane.

breakup. The VoF-based scheme is geometric and un-split, and exactly conserves mass. The entire methodology is developed in the setting of unstructured grids, allowing the accurate body-fitted treatment of complex geometries. As a demonstration of the unstructured capability, liquid atomization in swirling crossflow was simulated for a high-shear swirling injector. At first, the simulations were performed on a 30-degree sector of the swirling injector with one inlet jet to reveal the details of primary atomization and small-scale droplet breakup. The grid adaptation near the injector and the liquid jet structure are presented in this paper. For validation of our method, numerical simulations on the full circumference of the injector with six inlets were conducted in order to compare to UTRC experimental data. In the near field from the injector, the characteristics of liquid jet are qualitatively well compared with experimental images. For quantitative comparison, the droplet statistics at the downstream of the injector is compared with the experimental measurement. The droplet statistics including fuel mass flux and SMD from the simulations have good agreement with the experimental data. The present study shows that the Lagrangian stochastic breakup model works well even with the coarse grid in predicting droplet distributions. Considering that the computational cost would be problematic in most of practical cases since the Weber number is typically large, the present results demonstrate the capability of high-fidelity simulation for applications in a gas turbine or other combustion devices.

6 Acknowledgement

This work is supported by NAVAIR SBIR program under grant number N68335-11-C-0446. The authors acknowledge the valuable discussions with Dr. John T. Spyropoulos.

References

[1] J. J. Riley and G. S. Patterson. *Phys. Fluids*, 17(2):292–297, 1974.

[2] K. D. Squires and J. K. Eaton. *Phys. Fluids A: Fluid Dynamics*, 2(7):1191–1203, 1990.

[3] S Elghobashi and G C Truesdell. *J. Fluid Mech.*, 242:655–700, 1992.

[4] S. V. Apte, M. Gorokhovski, and P. Moin. *Int. J. Mult. Flow*, 29:1503–1522, 2003.

[5] Mark Sussman, Peter Smereka, and Stanley Osher. *J. Comp. Phys.*, 114(1):146–159, 1994.

[6] Denis Gueyffier, Jie Li, Ali Nadim, Ruben Scardovelli, and Stphane Zaleski. *J. Comp. Phys.*, 152(2):423 – 456, 1999.

[7] M. Herrmann. *J. Comp. Phys.*, 227:2674–2706, 2008.

[8] M Sussman, K. M. Smith, M. Y. Hussaini, M. Ohta, and R. Zhi-Wei. *J. Comp. Phys.*, 221:469 – 505, 2007.

[9] D Kim, F. Ham, M. Herrmann, and H. Le. *26th ILASS-Americas Conference, Portland, Oregon*, 2014.

[10] X. Li, M. C. Soteriou, W. Kim, J. M. Cohen, M. Herrmann, F. Ham, D. Kim, H. Le, and J. T. Spyropoulos. *presented at the ASME Turbo Expo 2013: Turbine Technical Conference and Exposition Volume 1B: Combustion, Fuels and Emissions, San Antonio, Texas*, GT2013-96000, 2013.

[11] C. Crowe, M. Sommerfeld, and Y. Tsuju. *Multiphase flows with Droplets and Particles*. CRC Press, Boca Ranton, FL., 1998.

[12] B.E. Gel'fand, S.A. Gubin, S.M. Kogarko, and S.P. Kormar. *J. Eng. Phys.*, 25:1140–1142, 1975.

[13] M. Pilch and C.A. Erdman. *Int. J. Multiphase Flow*, 13:741–757, 1987.

[14] M. Herrmann. *J. Comp. Phys.*, 229:745–759, 2010.